

Thin film deposition of tetrahedral amorphous carbon: a molecular dynamics study

N.A. Marks*

School of Physics A28, The University of Sydney NSW 2006, Australia

Available online 8 January 2005

Abstract

Molecular dynamics simulations of carbon thin film deposition are performed using the Environment Dependent Interaction Potential. Films deposited with carbon beams in the range 1–100 eV reproduce the energy dependence of the biaxial stress, density and tetrahedral bonding fraction observed experimentally. The transition from low-density, graphite-like amorphous carbon to the high-density tetrahedral phase occurs at an energy at which impacting ions do not penetrate the surface of the film. This result is incompatible with the generally accepted subplantation explanation for the diamond-like properties, and a new model of energetic burial is deduced from the simulations. Radial distribution functions compare well with experiment, and represent a significant improvement over Tersoff and Brenner simulations which contain unphysical distances.

© 2005 Elsevier B.V. All rights reserved.

PACS: 61.43.Bn; 81.15.Aa; 81.05.Uw

Keywords: Tetrahedral amorphous carbon; Amorphous carbon; Simulation; Ion beam deposition

1. Introduction

Tetrahedral amorphous carbon (ta-C) is an industrially useful diamond-like material prepared as a thin film using energetic ion beams [1–5]. Formation of ta-C is associated with an energy range of approximately 30–500 eV, and within this window ta-C has a tetrahedral bonding (sp^3) fraction as high as 80–85%, large compressive stresses (5–10 GPa) and a density of 3 g/cm³. Outside of the energy window amorphous carbon (a-C) is found, characterized by low stress, low-density structures and a predominance of graphite-like (sp^2) bonding.

Despite over a decade of investigation into ta-C, there remains ongoing debate over the nature of the process responsible for the high sp^3 fraction. The generally accepted subplantation model [6–8] attributes densification, compressive stress and the high sp^3 fractions to shallow implantation of energetic ions, while the cylindrical thermal spike model

suggests a temperature induced mobility process [9]. Other models propose a pressure-induced mechanism of sp^3 promotion arising from either compressive stress [1,10] or peening effects during energetic impact [11]. The theoretical uncertainty surrounding ta-C arises in part from experimental variability [9] associated with deposition and characterization, giving computational studies an important role. Molecular dynamics is the ideal tool for resolving the sp^3 question and other deposition issues, but modeling thin film growth is itself a formidable challenge requiring simulations with $\sim 10^3$ atoms running for $\sim 10^6$ timesteps. This computational burden has prevented the most accurate techniques such as density functional theory and non-orthogonal tight-binding from simulating film growth, and these methods have instead been applied in liquid-quench simulations at fixed density [12–16].

Empirical potentials have the computational efficiency required to model thin film growth, but typically the calculations have been limited by the transferability of the potential. Deposition simulations using the Tersoff potential [17] produced films which were neither ta-C nor a-C, having a density of 3 g/cm³ but an sp^3 fraction less than 30%

* Tel.: +61 293518167; fax: +61 293517726.

E-mail address: nigel@physics.usyd.edu.au.

[18,19]. Jäger and co-workers [19,20] deposited films using the Brenner potential [21] and these were found to have even lower sp^3 fractions than the Tersoff calculations, while high sp^3 content films deposited using a modified Brenner potential contained unphysical structures and distances. Similar anomalous features were observed in 100 eV orthogonal tight-binding simulations using a truncated cutoff [22]. The most successful simulations of ta-C deposition have used the Environment Dependent Interaction Potential (EDIP) [23]. These calculations [24,25] reproduce the transition from a-C to ta-C with increasing energy, anomalous distances are absent, and post-deposition implantation reproduces the energy window effect [25]. Somewhat controversially, the EDIP simulations found that films grown with beam energies of ~ 10 eV can have a density approaching 3 g/cm^3 , an sp^3 fraction greater than 50% and a large compressive stress—all the hallmarks of ta-C. This finding has significant implications for models of ta-C formation, and brings the accuracy and applicability of EDIP deposition under close scrutiny.

In this article we report on a significant set of details of the EDIP simulations which have not been previously presented. The procedure for depositing the EDIP films is explored carefully, and issues such as nucleation of the steady-state, identification of the bulk region and subplantation characterization are addressed. Analysis of the surface and bulk regions of the simulated films are shown to agree with experiment, and impact classification provides quantitative insight into the deposition of ta-C. Additional simulations are also performed in which EDIP is modified to increase its resemblance to the Tersoff and Brenner methods, and these calculations help explain some of the limitations of these methods for the simulation of ta-C.

1.1. Film growth models

Theoretical descriptions of the ta-C formation process have sought to explain three principal properties: compressive stress, density and sp^3 fraction. Experiments show that all three quantities are maximal in the same energy window, and share the same energy dependence [2]. Other materials also show an energy window for the compressive stress (e.g. TiN [26] and SiO_2 [27]), and thus theories of stress generation have an applicability beyond the amorphous carbons. The four principle explanations for ta-C are illustrated schematically in Fig. 1, and are discussed below.

1.1.1. Subplantation

This is the generally accepted explanation for the properties of ta-C, and has been proposed variously by Lifshitz [6], Davis [7] and Robertson [8]. In this model shallow implantation of energetic species is considered to generate a density increment in the sub-surface layers of the film, leading to sp^3 promotion and compressive stress.

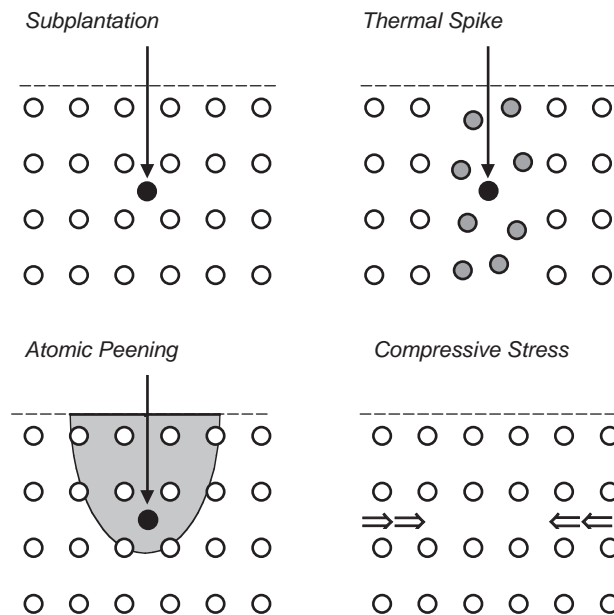


Fig. 1. Schematic illustration of popular models of ta-C thin film growth. The subplantation mechanism is attributed to Lifshitz [6], Davis [7] and Robertson [8], while the peening, thermal spike and compressive stress models are proposed by Koponen [11], Hofsäss [9] and McKenzie [10] respectively.

Experiment [28] and simulation [18,29] concur that surface penetration occurs with ions with energies greater than 30–40 eV, and thus a prediction of the subplantation model is that films with high-density, compressive stress and large sp^3 fractions should only occur above this energy.

1.1.2. Thermal spike

Hofsäss et al. [9] proposed a cylindrical thermal spike model in which the transient heating generated by ion impact leads to atomic rearrangements which favor the diamond-like properties of ta-C. Using analytic models of heat diffusion and ion implantation statistics from binary collision calculations, they predict ta-C formation between energies of 50 eV and 2 keV. This model lies in opposition to conventional understanding of energetic beam deposition where thermal spikes are considered a mechanism for annealing, leading to stress relief, reduction in density reduction and lower sp^3 fractions.

1.1.3. Compressive stress

Under high-pressure (~ 4 GPa) graphite will transform to diamond at room temperature and McKenzie et al. [1,10] have suggested that the compressive stress generated during film growth could be responsible for the high sp^3 phase. This model draws upon thermodynamics, and is suggestive of a threshold process, and thus the compressive stress explanation would suggest that the sp^3 fraction has a non-linear dependence on the stress. Due to experimental uncertainty it has not been possible to quantitatively determine this relationship.

1.1.4. Atomic peening

A thermodynamic process was also put forward by Koponen et al. [11] who proposed that ion impact leads to a transient high-pressure phase leading to sp^3 bonding. This “peening” model of ta-C is differentiated from the compressive stress in that the high pressure is intrinsically associated with impact rather than imposed externally by the existing film. In the case of ta-C deposited using mass-selected ion beam this model describes the entire energy dependence with just two parameters: a displacement energy, and an exponential relaxation component.

1.2. Deposition methodology

The interatomic interactions are described using the Environment Dependent Interaction Potential (EDIP) first proposed for silicon [30] and recently generalized for carbon [23]. Carbon EDIP captures important π -repulsion terms absent in potentials such as Tersoff, Brenner and orthogonal tight-binding, and is well-suited to modeling thin film deposition as its analytic form is computationally efficient, while its transferability properties are good for an empirical potential. The functional form of EDIP consists of three components: a two-body pair energy, a three-body angular penalty and a generalized coordination. The two- and three-body terms have environment dependence controlled by the atomic coordination Z which in general has a fractional value. The coordination is decomposed into a spherical contribution z_i and an aspherical term unique to the carbon potential which is vital for describing distorted configurations involving π -electrons. The importance of these π -repulsion terms is illustrated in additional simulations performed in this work in which the π -terms are set to zero, and the coordination cutoffs are reparametrized to reproduce the switching functions of the Tersoff and modified Brenner potentials. These calculations highlight the errors which occur when the non-bonding terms are neglected.

The films were grown using monoenergetic beams, with each film deposited onto a room temperature (001) diamond substrate with (2×1) reconstructed upper and lower surfaces. Periodic boundary conditions were applied in the x and y -directions, each with a side length of 14.22 Å. For each energy at least five hundred atoms are deposited sequentially onto the upper surface with normal incidence and random position in the xy -plane. Each impact is allowed to fully equilibrate prior to subsequent impact. In excess of ten films were deposited, with energies ranging from 1 eV up to 100 eV.

The impact of an energetic species leads to substantial heating of the substrate and film, and thus velocity rescaling wall thermostats of thickness 2 Å acted upon atoms with a lateral displacement greater than 6.11 Å from the initial position of the incident atom. These thermostats prevent recycling of energy through the boundaries, and a similar thermostat applied to the substrate base removes

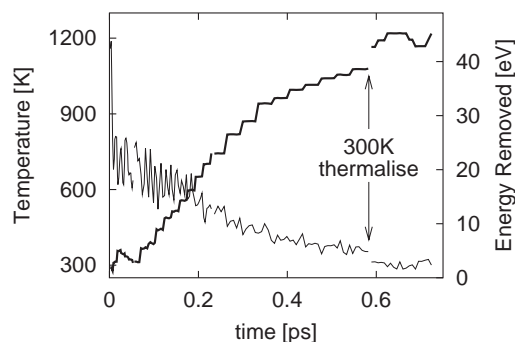


Fig. 2. System temperature (thin line) and energy removed by wall and base thermostats (thick line) as a function of time after the impact of a 40 eV atom onto a 384-atom substrate initially at 300 K and thermostatted to the same temperature.

heat which would diffuse away were the system infinite. The motion of all atoms was typically followed for 0.6 ps, and rethermalization to 300 K was carried out prior to deposition of the subsequent atom. This scheme is demonstrated in Fig. 2, where it is apparent that 0.6 ps is sufficient time for the kinetic energy from the 40 eV impact to disperse through the film/substrate, and then diffuse to the boundaries where it is extracted. Note that this method necessarily approximates the experimental situation where the time between successive impacts is in the order of a millisecond, and thus the simulation specifically excludes thermally activated diffusion processes which might potentially contribute to increased surface graphitization.

2. Results

The deposited carbon films were analyzed with a variety of characterization techniques to categorize surface structure, bulk properties and steady-state growth modes. All the films were found to be amorphous and to possess a low-density π -bonded surface, while large variations were found in the properties of the bulk region. Here the energy of the deposition beam was found to strongly influence important material properties such as density, sp^3 fraction and biaxial stress. Fig. 3 provides an excellent example of the dramatic changes in morphology and structure which are driven by the beam energy. In the left-hand panel the 1 eV beam generates a low-density film containing mostly sp^2 -bonded atoms (blue circles), while in the film deposited with a 70 eV beam the majority of the atoms are sp^3 bonded (red circles) and the density is noticeably higher. This energy-induced transition from a low-density, sp^2 -rich material, to a high-density, sp^3 -rich material is one of the key experimental results in the amorphous carbon literature and represents one of the key achievements of these EDIP film growth simulations. In being able to successfully model energetic carbon deposition EDIP thus enables for the first time a confident analysis and characterization of the sp^3

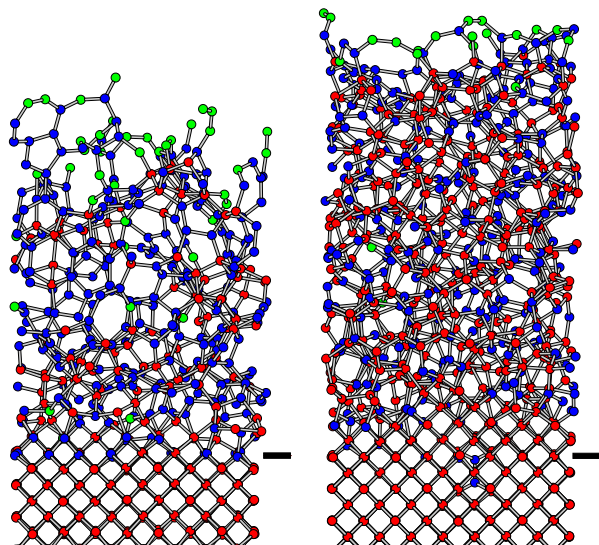


Fig. 3. Carbon thin films deposited with 1 eV atoms (left) and 70 eV atoms (right). Coordination determined by counting neighbors within 1.85 Å, with green, blue and red circles denoting atoms with two, three and four neighbors respectively. The horizontal bars indicate the initial height of the respective substrates. (For interpretation of the references to colour in this figure legend, the reader is referred to the web version of this article.)

generation mechanism and the amorphous carbon formation process in general.

2.1. Steady-state growth

In recent simulations using the Tersoff and Brenner potentials, Jäger and Albe [19] found that steady-state growth was not achieved even after several hundred atoms had been deposited. While their deposition details differ to those of this work, it nonetheless raises the question of what system size must be simulated before a realistic description of bulk material is achieved. To assess the nature of steady-state growth in these EDIP calculations we followed the method of Jäger and Albe and graphed the number of sp^2 and sp^3 atoms in the system as a function of the number of atoms added to the system. Note that the latter quantity specifically excludes sputtered atoms, and therefore is not the same as the number of atoms deposited.

Fig. 4 presents the number of sp^3 atoms as a function of atoms added, and demonstrates that for energies up to 40 eV the number of sp^3 sites increases linearly with the number of additional atoms, indicating steady-state growth. The gradient of the fitted line corresponds to the coordination fraction and increases with energy as seen earlier in Fig. 3. Identical conclusions are reached using similar plots for the sp^2 sites. For the 70 and 100 eV films the 0.6 ps data (circles) are not fitted by a single straight line, but instead undergo a change in slope after several hundred atoms. This indicates a change in growth mode in which fewer sp^3 sites are generated, as seen in the reduction in slope. Inspection of the simulations revealed that the initially high slope reflected a period of epitaxial growth in which the crystalline structure

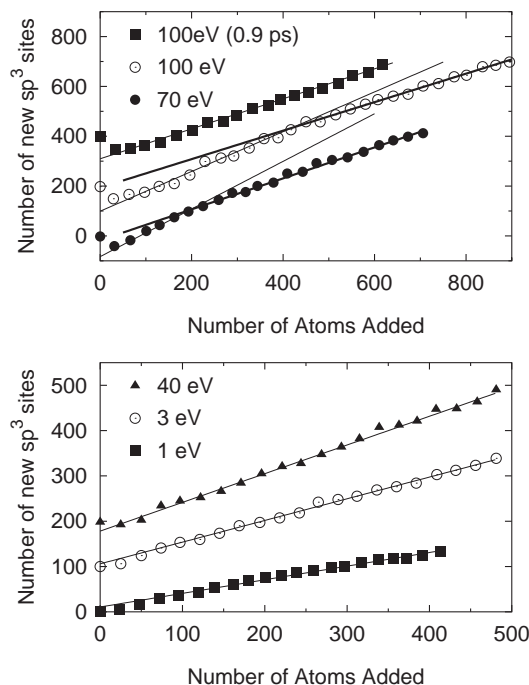


Fig. 4. Number of new sp^3 sites as a function of additional atoms. The straight lines are fits to the data to demonstrate steady-state growth. For clarity, the various data-sets are vertically offset by multiples of 100 or 200. Most calculations used 0.6 ps thermal spikes, with the exception of the 100 eV data denoted by squares where motion was followed for 0.9 ps.

of the substrate expanded upwards. This effect is visible in the right-hand panel of Fig. 3 where the (001) channels are seen to continue above the horizontal bar indicated the original substrate surface. This semi-crystalline growth mode cannot continue indefinitely however, as the slope of the sp^3 data in Fig. 4 is less than unity (approximately 0.80), and thus the amorphous film continues to increase in thickness. Consequently, a critical point is reached at which the crystalline–amorphous interface lies beyond the range of the energetic atoms and the growth mode converts to the generation of a purely amorphous phase. Once this point has been reached, we have nucleated the amorphous phase, and thus begin the steady-state growth.

The onset of the change in growth mode is demonstrated in Table 1 which quantifies this two-stage growth

Table 1
Influence of thermal spike duration on evolution of the high energy films

Quantity	Property	70 eV (0.6 ps)	100 eV (0.6 ps)	100 eV (0.9 ps)
sp^3 fraction	Initial slope	81	79	
	Final slope	61	57	60
	Transition	278	420	
sp^2 fraction	Initial slope	20	18	
	Final slope	38	43	39
	Transition	277	403	

Units follow according to Fig. 4, with the intercept given in atoms, and the coordination fractions determined from the various gradients and expressed as a percentage.

mode. For both calculations using ~0.6 ps thermal spikes, the initial gradient is almost exactly the average of the sp³ fraction of the amorphous phase and the 100% value corresponding to fully epitaxial growth, thus indicating a 50:50 mix between the two phases. The third column of the table records the properties of an additional calculation performed using 100 eV impacts. For this film the deposition conditions (including the pseudo-random numbers used to select impact sites) were identical except for an increase in the thermal spike lifetime to 0.9 ps. As shown in Fig. 4, this change leads to the amorphous phase being nucleated almost immediately, and no epitaxial growth is generated. Significantly, the sp³ creation rate for the 0.9 ps film is extremely close to the value for the 0.6 ps once amorphous nucleation was initiated. This demonstrates that once amorphous material is being formed in a steady-state process, the structure is well-defined and properties can be computed with confidence.

2.2. Properties of the bulk

The steady-state analysis of the previous section is useful for computing coordination fractions, but it cannot be applied to the calculation of properties such as density, stress and radial distribution function. For these types of quantities we require cutting planes which select the bulk region of the system—that is, the region which is undergoing steady-state growth, and would eventually come to dominate the entire system in the limit of an infinitely thick film. The approach adopted here uses an analytic fitting function applied to the coordination profile of sp³ sites as a function of vertical distance z . As shown in Fig. 5, for negative values of z the sp³-coordination is 100%, this being the substrate region, while for small positive values of z the fraction of sp³ sites is constant as this is the bulk region of the film which is undergoing steady-state growth. For the highest values of z the fraction of sp³ sites falls to zero as the surface is dominated by chains and loops consisting of sp and sp² sites only (Fig. 3). This general trend is typical of all films considered in this study, regardless of deposition

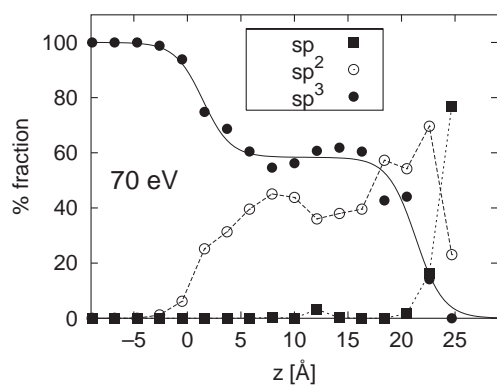


Fig. 5. Coordination fractions as a function of depth (z) for the 70 eV film. The solid line indicates the analytic fit used to identify the bulk region, and the original height of the substrate corresponds to $z=0$.

Table 2

Comparison of properties determined using steady-state analysis (Fig. 5) and bulk analysis

Quantity	Energy (eV)										
	1	2	2.5	3	6	8	10	25	40	70	100
<i>sp³ fraction (%)</i>											
Bulk	33	36	43	48	57	54	55	57	59	58	56
Gradient	30	33	42	48	58	56	57	57	63	61	57
<i>sp² fraction (%)</i>											
Bulk	64	61	54	51	42	46	45	43	41	41	44
Gradient	65	61	55	51	43	42	44	42	37	38	43

energy, and thus we define the bulk region using the density profile $n(z)$ given by

$$n(z) = \frac{100 - f}{\exp[(z - z_{\min})/w] + 1} + \frac{f}{\exp[(z - z_{\max})/w] + 1}$$

where $z_{\min}+3w$ and $z_{\max}-3w$ define the lower and upper bounds of the bulk region, f is the fraction of sp³ sites in the bulk, and w is a characteristic width of interfaces. While this expression could be generalized to have two different values of w (one for the substrate–film interface, and a second for the free surface), it was found that a single w parameter greatly increased the robustness of the non-linear fit. The suitability of the analytic fitting function for identifying the bulk region is benchmarked in Table 2. The data labeled ‘Bulk’ denote coordination fractions determined by counting the coordination of atoms residing within the bulk region, and the values compare well with the steady-state values.

Having established a robust and reliable method for identifying the bulk region of the thin films, it is now possible to compute a variety of material properties. Fig. 6

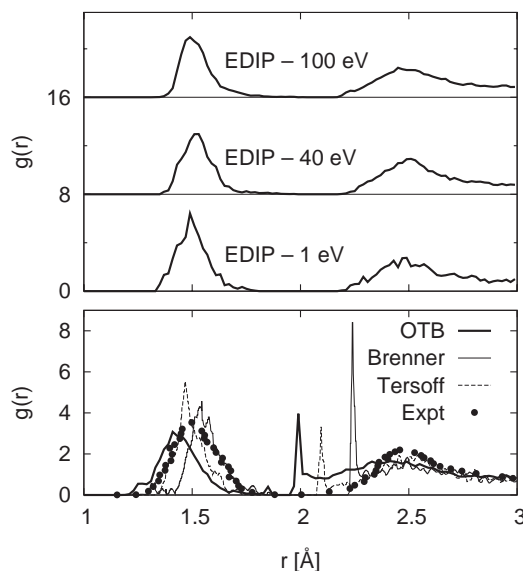


Fig. 6. Radial distribution function $g(r)$ for the bulk region of various EDIP films. The experimental data are neutron diffraction data from Gilkes [31], the Tersoff and modified Brenner data are from deposition simulations by Jäger and Albe [19], while the orthogonal tight-binding (OTB) calculations are from Cooper et al. [22].

shows the radial distribution function (RDF) for the bulk region of several EDIP films. The EDIP second neighbor distances compare well with neutron diffraction data [31], while the first neighbor peaks are a bit narrower, in most part due to the presumption of graphite-like conjugation for sp^2 sites. This difference is minor compared to the spurious peaks in the three simulation sets shown in the lower panel of Fig. 6. These unphysical spike in the RDF fall in-between the first and second neighbors, and in each case the position of the spike coincides with the interaction cutoff of the corresponding potential. While not wishing to overstate the point, this kind of feature should not be overlooked, as it represents an unphysical metastable structure intermediate between sp^2 and sp^3 bonding. The origin of these structures is considered in a later section using EDIP calculations with modified and truncated interactions.

Fig. 7 presents the energy dependence of the EDIP films for the sp^3 fraction, density and biaxial stress. As observed experimentally, increasing the deposition energy leads to a dramatic change in material properties. At low energies the films have all the hallmarks of a-C, possessing a low-density, tensile stress and predominantly sp^2 bonding (the sp fraction is only 1%). The EDIP film deposited at 1 eV compares particularly favorably with experimental studies of a-C by Li and Lannin [33]. Analysis of their experimental RDF yielded an experimental density of 2.44 g/cm^3 , an average bondlength of 1.46 \AA and an average coordination of 3.34 (using a cutoff of 1.90 \AA). In comparison, the EDIP film at 1 eV has a

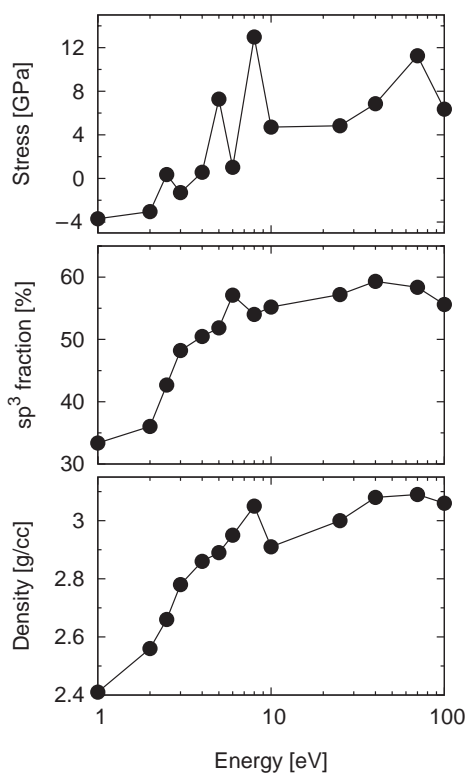


Fig. 7. Variation in stress [32], sp^3 fraction and density for carbon thin films deposited with EDIP. All properties are computed for the bulk region as defined by the analytic fitting function shown in Fig. 5.

density of 2.41 g/cm^3 , an average bondlength of 1.49 \AA and an average coordination of 3.32 (for a cutoff of 1.85 \AA). These EDIP calculations also compare well to higher-level simulations using orthogonal tight-binding [34] which also find similar sp^3 fractions to those reported here. In contrast, Tersoff simulations of a-C found only 6% sp^3 bonding and an average coordination of 2.84 [18].

At the highest energies considered here, the film properties have the signature of ta-C, that is, high-density, large compressive stress and predominantly sp^3 bonding. The density and stress values compare extremely well to experimental data in the literature, while the EDIP sp^3 values are lower than most experimental values which are typically 80–85%. This underestimation of sp^3 fractions at high density is a limitation of EDIP which has been illustrated in liquid-quench simulations [35] and thus the behavior here is to be expected. Another simulation shortcoming is the small system size which leads to large fluctuations in the compressive stress from one impact to the next. To reduce uncertainty, the film properties were averaged over multiple configurations, but even with these measures, considerable variability is still present, as visual inspection of Fig. 7 shows.

Despite these technical aspects, the overall picture in Fig. 7 of the transformation from a-C to ta-C is clearly apparent, and when taken in combination with the physical RDFs of Fig. 6 and the absence of five-fold coordination, there can be confidence that EDIP is capturing the essence of thin film carbon deposition. The only controversial aspect is the energy at which the transformation occurs. Although Lossy et al. [3] found ta-C production around 7 eV, the standard literature value for the ta-C threshold is 30–40 eV. To help address this issue it is necessary to consider the nature of the film growth, which is the subject of the following section.

2.3. Film growth mechanism

One of the unique possibilities provided by molecular dynamics the potential to view atomic-scale information and thus gain insight into thin film processes. That said, the analysis of amorphous thin film growth is highly non-trivial, and even the seemingly simple act of defining the surface is highly problematic, and one is forced to adopt a metric [18,20] and work within that framework.

In previous EDIP calculations [25] we have used the method proposed by Kaukonen and Nieminen [18], and in agreement with experiment [28] and simulation [18,29], subplantation was found to commence around 40 eV. This agreement with other sources gives confidence that the EDIP interactions are physical and reasonable. Having established this point, the results of Fig. 7 are then clearly inconsistent with the subplantation model [6–8] as ta-C is produced for energies significantly under the subplantation threshold. The compressive stress model [10] is also not consistent with the simulations, as the sp^3 fraction and density do not have the required non-linear dependence on

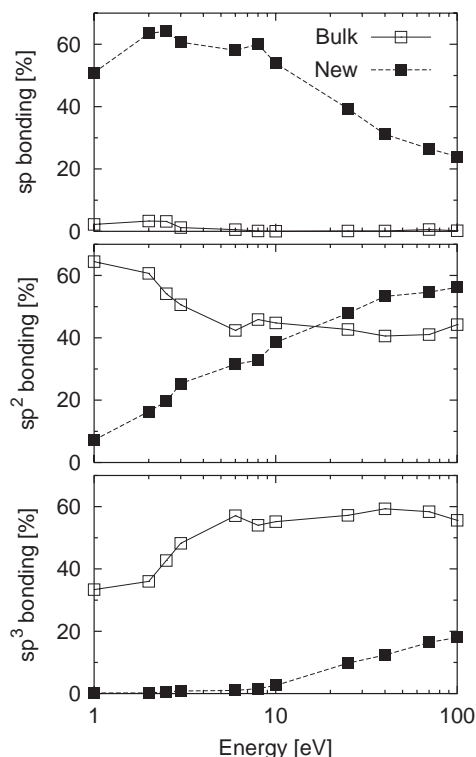


Fig. 8. Coordination classification for newly deposited atoms (expressed as a percentage of all impacts and shown with solid squares), and atoms in the steady-state bulk region (expressed as a percentage of all atoms in the bulk and show as white squares).

the compressive stress. This conclusion is supported by recent experiments [36] in films with high sp^3 fractions that were deposited with comparatively low stresses of ~ 2 GPa. Furthermore, the presence of ta-C for EDIP energies of ~ 10 eV is clearly incompatible with the thermal spike model [9], since an impact of such low energy can break only a bond or two, which is by no means a liquid-like state as typically envisioned in a spike.

Of the four models discussed earlier, we are left with the “peening” model of Koponen et al. [11] which proposes that a high-pressure pulse leads to sp^3 creation. Evidence in support of the peening model is shown in Fig. 8 which compares the coordination of atoms in the bulk with the environment of newly deposited atoms (that is, after thermalization as seen in Fig. 2 but prior to subsequent impact). The solid squares show that the vast majority of newly arrived atoms locate in surface sites, with two-fold sp sites the most common environment below 25 eV. In contrast, newly arrived atoms are rarely deposited into sp^3 sites, although for energies above 5 eV the sp^3 fraction of bulk sites exceeds 50%. The unavoidable conclusion is that depositing atoms change the hybridization of existing atoms, converting sp sites to sp^2 , and sp^2 sites to sp^3 . This process therefore is one of energetic burial (or peening), in which the pressure pulse generated during impact generates new bonds and increases the coordination number. This three-dimensional growth model is reminiscent of a surface

insertion model developed from two-dimensional Stillinger–Weber simulations of carbon film growth [37]. In these calculations compressive stress was generated without subplantation, a process repeated here in three dimensions. In a further analogy with the current work, the 2D bulk stresses were compressive while the surface layers were under tension [24], and it was only the action of burial during energetic impact which promoted the transformation to a compressive phase.

2.4. The importance of π interactions

Having demonstrated the usefulness of EDIP in simulations of carbon thin film growth, it is instructive to consider calculations in which the various π interactions (bonded and non-bonded) are disabled and/or reparameterized. This approach provides insight into the effect of the terms in the potential, and helps to explain behavior such as the low sp^3 fractions producing some potentials, and spurious RDF features seen in Fig. 6.

Table 3 lists the results of six film deposition simulations performed at 40 eV. The calculations fall into two groupings and will be discussed in turn. The first set of calculations are full and partial EDIP calculations where the only difference between the calculations is the omission of specific terms. Whereas the first calculation is the full model as presented in this work, the second calculation has the non-bonded π -repulsion interaction set to zero. The third calculation has both the π -repulsion and the dihedral penalty term set to zero, and in this form the potential contains only spherical coordination counting as in the original EDIP for silicon [30]. Comparison of the sp^3 fractions for the three EDIP calculations shows the crucial importance of the π interactions for the simulation of ta-C. When both the dihedral interaction (a bonding term) and the π -repulsion (a non-bonding term) are set to zero, the structure collapses into a highly (89%) sp^2 configuration with an unphysically high density (graphite has a density of 2.27 g/cm³). When the dihedral interaction is activated (but non-bonding terms are still absent), the sp^2 sites exhibit increased local planarity, which removes entropic freedom of the sp^2 sites and thus increases the sp^3 fraction. However, in the absence of non-bonded repulsion, graphite-like regions can still pack into

Table 3

Properties of films deposited with a 40 eV beam using the full EDIP potential, and various simplified and modified forms of EDIP as discussed in the text

	sp^2 (%)	sp^3 (%)	Density (g/cm ³)	Stress (GPa)
Full EDIP model	40	59	3.08	6.9
EDIP (no non-bonding term)	59	41	3.10	9.4
EDIP (no π -terms)	89	10	3.19	29
Tersoff-like (2.10 Å cutoff)	94	4	3.59	8.0
Brenner-like (2.10 Å cutoff)	57	36	3.33	4.5
Brenner-like (2.25 Å cutoff)	42	56	3.16	14
Experiment	15–40	60–85	3.0–3.1	5–10

artificially dense configurations, and so it is only with the full EDIP model that the driving force for sp^3 generation is finally realized, and agreement with experiment is obtained.

The second set of simulations involve some reparametrization of EDIP to increase the resemblance with the Tersoff and Brenner potentials. The principle step is the modification of the EDIP spherical coordination counting function $f(r)$ (Eq. (8) in [23]) to accurately reproduce the half-cosine cutoff function used in both potentials. For the Tersoff-like simulations the parameters were (in the notation of [23]) $f_{\text{low}}=1.754 \text{ \AA}$, $f_{\text{high}}=2.304 \text{ \AA}$ and $\alpha=14.46$, which produces a cutoff which effectively goes to zero at 2.10 \AA as for the Tersoff method. The original Brenner potential [21] uses the same cutoff function as Tersoff, while the modified Brenner interaction by Jäger and Albe [19] uses a rigid shift to increase the cutoff to 2.25 \AA . For the latter calculations the same α is used as for the Tersoff-like calculations and f_{low} and f_{high} are each 0.15 \AA larger. Non-bonding interactions between π sites are absent in the Tersoff and Brenner potentials, and thus all three calculations in the second group have the non-bonded π -repulsion term set to zero. Dihedral interactions are absent in the Tersoff potential, but are included in the Brenner potential (where they are overestimated by $\approx 70\%$ as noted by Wu et al. [38]). To maximise the similarity with the Brenner potential, the quantity z_{dih} (as defined in [23]) was increased from its EDIP value of 0.30 to 0.65.

Having modified EDIP to make it as Tersoff-like and Brenner-like as possible [39], we can now discuss the film properties of the second group in Table 3. The Tersoff-like films bear the least resemblance to experiment, and the consequences of omitting dihedral and non-bonded repulsion interactions are similar to the third EDIP calculation which also lacked π -terms. Inclusion of the strong dihedral interaction for the first Brenner-like film (the one with the same cutoff as the Tersoff-like film) has a major effect. As for the EDIP system, the dihedral terms enforce local planarity of sp^2 sites which prevents unphysical three-dimensional folding of sp^2 regions. Increasing the cutoff for the Brenner-like does not have as large an effect as seen by Jäger and Albe [19], but the same general trend is seen in which sp^3 fractions increase and the (unphysically high) density is reduced. For completeness, it is interesting to note that an additional Brenner-like simulation using a 2.25 \AA cutoff and $z_{\text{dih}}=0.30$ as for EDIP produced a 3.12 g/cm^3 film with an sp^3 fraction of 41%, thus confirming the influence of the Brenner dihedral interaction on the diamond-like properties.

The relationship between the RDF and selected reparametrizations of EDIP is shown in Fig. 9 which presents data for the Tersoff-like simulation and the EDIP simulation without any π -terms. As seen earlier (Fig. 6), the Tersoff-like simulation (dotted lines) has a significant spike at the interaction cutoff of 2.10 \AA . The Brenner-like simulation with a 2.10 \AA cutoff exhibits a similar spike, but for the 2.25 \AA Brenner-like calculation this spike is markedly smaller, and is similar to the EDIP calculation without π -terms (thick lines)

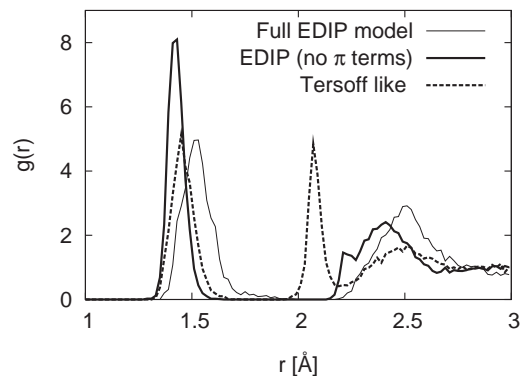


Fig. 9. Radial distribution function $g(r)$ for the bulk region of 40 eV films selected from Table 3 as indicated by the legend.

for which the cutoff is 2.27 \AA . From this behavior we can empirically conclude that increasing the cutoff function reduces metastable configurations between the first and second neighbor shells. However, for a robust and reliable treatment of these intermediate distances, the preferred solution is as indicated in the derivation of EDIP [23,24], in which *ab initio* data of bond making and breaking are used to determine the parameters and functional form of the cutoff function.

3. Conclusion

The simulations in this work successfully model the thin film deposition of a-C and ta-C due to the presence of dihedral and non-bonded π -repulsion terms in the interatomic potential. Densities, sp^3 fractions and stresses correlate with the incident energy as observed experimentally, and no unphysical distances or coordinations are present. The subplantation model is inconsistent with the simulations which find ta-C growth commencing below 10 eV. A model of ta-C film growth is proposed based upon the principle of surface insertion in which energetic burial leads to the simultaneous processes of sp^3 promotion, densification, stress generation and surface growth.

References

- [1] D.R. McKenzie, D. Muller, B.A. Pailthorpe, *Phys. Rev. Lett.* 67 (1991) 773.
- [2] P.J. Fallon, V.S. Veeraramy, C.A. Davis, J. Robertson, G.A.J. Amaratunga, W.I. Milne, J. Koskinen, *Phys. Rev., B* 48 (1993) 4777.
- [3] R. Lossy, D.L. Pappas, R.A. Roy, J.P. Doyle, J.J. Cuomo, J. Bruley, *J. Appl. Phys.* 77 (1995) 4750.
- [4] Y. Lifshitz, *Diamond Relat. Mater.* 5 (1996) 388.
- [5] S.R.P. Silva, S. Xu, B.X. Tay, H.S. Tan, W.I. Milne, *Appl. Phys. Lett.* 69 (1996) 491.
- [6] (a) Y. Lifshitz, S.R. Kasi, J.W. Rabalais, *Phys. Rev. Lett.* 68 (1989) 1290;
(b) Y. Lifshitz, S.R. Kasi, J.W. Rabalais, W. Eckstein, *Phys. Rev., B* 41 (1990) 10468.
- [7] C.A. Davis, *Thin Solid Films* 226 (1993) 30.
- [8] (a) J. Robertson, *Diamond Relat. Mater.* 2 (1993) 984;
(b) J. Robertson, *Diamond Relat. Mater.* 3 (1994) 361.

- [9] H. Hofsässs, H. Feldermann, R. Merk, M. Sebastian, C. Ronning, *Appl. Phys.*, A 66 (1998) 153.
- [10] D.R. McKenzie, *Rep. Prog. Phys.* 59 (1996) 1611.
- [11] I. Koponen, M. Hakovirta, R. Lappalainen, *J. Appl. Phys.* 78 (1995) 5837.
- [12] (a) N.A. Marks, D.R. McKenzie, B.A. Pailthorpe, M. Bernasconi, M. Parrinello, *Phys. Rev. Lett.* 76 (1996) 768;
(b) N.A. Marks, D.R. McKenzie, B.A. Pailthorpe, M. Bernasconi, M. Parrinello, *Phys. Rev.*, B 54 (1996) 9703.
- [13] D.G. McCulloch, D.R. McKenzie, C.M. Goringe, *Phys. Rev.*, B 61 (2000) 2349.
- [14] D.A. Drabold, P.A. Fedders, P. Stumm, *Phys. Rev.*, B 49 (1994) 16415.
- [15] U. Stephan, Th. Frauenheim, P. Blaudeck, G. Jungnickel, *Phys. Rev.*, B 50 (1994) 1489.
- [16] (a) C.Z. Wang, K.M. Ho, *Phys. Rev. Lett.* 71 (1993) 1184;
(b) C.Z. Wang, K.M. Ho, *Phys. Rev.*, B 50 (1994) 12429.
- [17] J. Tersoff, *Phys. Rev. Lett.* 61 (1988) 2879.
- [18] (a) H.-P. Kaukonen, R.M. Nieminen, *Phys. Rev. Lett.* 68 (1992) 620;
(b) M. Kaukonen, R.M. Nieminen, *Phys. Rev.*, B 61 (2000) 2806.
- [19] H.U. Jäger, K. Albe, *J. Appl. Phys.* 88 (2000) 1129.
- [20] H.U. Jäger, A.Yu. Belov, *Phys. Rev.*, B 68 (2003) 024201.
- [21] (a) D.W. Brenner, *Phys. Rev. Lett.* 42 (1990) 9458;
(b) D.W. Brenner, *Phys. Status Solidi B* 217 (2000) 23.
- [22] N.C. Cooper, M.S. Fagan, C.M. Goringe, N.A. Marks, D.R. McKenzie, *J. Phys.: Condens. Matter* 14 (2002) 723.
- [23] N.A. Marks, *Phys. Rev.*, B 63 (2001) 035401.
- [24] N.A. Marks, *J. Phys.: Condens. Matter* 14 (2002) 2901.
- [25] N.A. Marks, J.M. Bell, G.K. Pearce, D.R. McKenzie, M.M.M. Bilek, *Diamond Relat. Mater.* 12 (2003) 2003.
- [26] H.H. Hoang, D.R. McKenzie, W.D. McFall, Y. Yin, *J. Appl. Phys.* 80 (1996) 6279.
- [27] A. Durandet, D.R. McKenzie, *J. Appl. Phys.* 80 (1996) 4707.
- [28] Y. Lifshitz, G.D. Lempert, E. Grossman, *Phys. Rev. Lett.* 72 (1994) 2753.
- [29] S. Uhlmann, Th. Frauenheim, Y. Lifshitz, *Phys. Rev. Lett.* 81 (1998) 641.
- [30] J.F. Justo, M.Z. Bazant, E. Kaxiras, V.V. Bulatov, S. Yip, *Phys. Rev.*, B 58 (1998) 2539.
- [31] K.W.R. Gilkes, P.H. Gaskell, J. Robertson, *Phys. Rev.*, B 51 (1995) 12303.
- [32] Note that the stresses here are 50% larger than those reported in earlier publications (e.g. [24,25]). This error arose from an incorrect scaling factor in the definition of the stress tensor.
- [33] F. Li, J.S. Lannin, *Phys. Rev. Lett.* 65 (1990) 1905.
- [34] K. Kohary, S. Kugler, *Phys. Rev.*, B 63 (2001) 193404.
- [35] N.A. Marks, N.C. Cooper, D.R. McKenzie, D.G. McCulloch, P. Bath, S.P. Russo, *Phys. Rev.*, B 65 (2002) 075411.
- [36] M. Bonelli, A.C. Ferrari, A. Fioravanti, A. Li Bassi, A. Miotello, P.M. Ossi, *Eur. Phys. J.*, B 25 (2002) 269.
- [37] N.A. Marks, D.R. McKenzie, B.A. Pailthorpe, *Phys. Rev.*, B 53 (1996) 4117.
- [38] C.J. Wu, J.N. Glosli, G. Galli, F.H. Ree, *Phys. Rev. Lett.* 89 (2002) 135701.
- [39] Note that EDIP still has a variable interaction range due to the parameter a' which cannot be set to zero without reparametrizing the entire potential.